# Comparative Analysis of Elliptical and Cylindrical Slot Tubes in Cross-Flow Radiators: Thermal Resistance and Flow Characteristics

Anand Pai, Satish Shenoy B., and Chandrakant R Kini\*

Abstract—Cross-flow heat exchangers are extensively employed in automotive radiators, where hot coolant flows through internal tubes while ambient air flows orthogonally across them. Conventional designs typically utilize flat tubes; however, this study investigates the thermal performance of alternative tube geometries-elliptical and cylindrical slot profiles-through a combination of analytical modeling and three-dimensional computational fluid dynamics (CFD) simulations. In this study, the influence of tube geometry on heat transfer effectiveness and thermal resistance of the heat exchanger under representative automotive operating conditions was assessed. Results indicated that elliptical tubes exhibit significantly lower total thermal resistance compared to cylindrical slot tubes, attributed to enhanced convective heat transfer characteristics. The CFD model, validated against analytical results, demonstrated strong agreement and highlighted the potential of elliptical geometries for improving thermal efficiency in next-generation radiator

Index Terms-Cross flow heat exchanger, Radiators, Tube geometry, Heat Transfer, Thermal Resistance.

#### NOMENCLATURE

|              | NOMENCLATURE   |
|--------------|--|
| A            | Cross-sectional area of RVE domain perpendicular               |
|              | to external flow (m <sup>2</sup> )                             |
| $A_c$        | Cross-sectional area of the tube flow domain (m <sup>2</sup> ) |
| C            | Empirical constant in Nusselt correlation                      |
| $D_h$        | Hydraulic diameter (m)   |
| $D_{h,o}$    | Hydraulic diameter for external flow (m)                       |
| F            | Correction factor for cross flow heat exchangers               |
|              | based on Bowman charts   |
| $Nu_i$       | Nusselt number (dimensionless)                                 |
| $Nu_o$       | Nusselt number for external flow (-)                           |
| $P_w$        | Wetted perimeter of the tube geometry (m)                      |
| $P_{w_i}$    | Wetted perimeter of the tube inner surface (m)                 |
| $P_{w_o}$    | Wetted perimeter of the tube outer surface (m)                 |
| $Pr_i$       | Prandtl number (dimensionless)                                 |
| $Pr_o$       | Prandtl number of air (–)                                      |
| $R_{cond,c}$ | Thermal Conductive Resistance of the flat faces of             |
|              | cylindrical slot tube (°C/W)                                   |
| $R_{cond,f}$ | Thermal Conductive Resistance of semicircular                  |
| ,,           | ends of cylindrical slot tube (°C/W)                           |
|              |  |

Manuscript received April 27, 2025; revised August 7, 2025.

A. Pai is an Associate Professor in the Department of Aeronautical and Automobile Engineering, Manipal Institute of Technology, Manipal Academy of Higher Education, Manipal, Karnataka, India, 576104. (e-mail: anand.pai@manipal.edu).

B.S. Shenoy is a Professor in the Department of Aeronautical and Automobile Engineering, Manipal Institute of Technology, Manipal Academy of Higher Education, Manipal, Karnataka, India, 576104. (e-mail: satish.shenoy@manipal.edu).

C.R. Kini is a Professor in the Department of Aeronautical and Automobile Engineering, Manipal Institute of Technology, Manipal Academy of Higher Education, Manipal, Karnataka, India, 576104 (corresponding author to provide phone: +91-8202925482; e-mail: chandra.kini@manipal.edu).

 $R_{cond,tot}$  Total Thermal Conductive Resistance of the cylindrical slot tube (°C/W)

Thermal Resistance of Wall conduction (°C/W)

 $R_{conv,i}$  Thermal Resistance of Internal convection (°C/W)

 $R_{conv,o}$  Thermal Resistance of External convection (°C/W)  $R_{tot,ellipse}$  Total Thermal Resistance of the elliptical tube

 $R_{tot,slot}$  Total Thermal Resistance of the cylindrical slot tube (°C/W)

Total Thermal Resistance of the tube (°C/W)  $R_{tot}$ 

Reynolds number (dimensionless)  $Re_i$ 

Reynolds number based on external (air) flow (-)  $Re_o$ 

UOverall heat transfer coefficient (W/m<sup>2</sup>/K)

Exponent of Reynolds number in Nusselt correlation  $\alpha$ 

β Exponent of Prandtl number in Nusselt correlation

 $\dot{Q}$  $\dot{V}$ Rate of heat transfer (W)

Volumetric flow rate of coolant (m<sup>3</sup>/s)

 $\dot{m_a}$ Mass flow rate of air (kg/s)

Mass flow rate of coolant (kg/s)  $\dot{m}$ 

 $\dot{m}_{\mathrm{tube}}$ Mass flow rate per tube (kg/s)

Heat flux across the cross flow heat exchanger  $\dot{q}_{cf}$  $(W/m^2)$ 

Dynamic viscosity of the fluid (Pa·s)  $\mu$ 

Dynamic viscosity of air (Pa·s)  $\mu_a$ 

Fluid density (kg/m<sup>3</sup>)

Density of air (kg/m<sup>3</sup>)

Logarithmic mean temperature difference (K)

Corrected temperature difference (K)

Aspect ratio of the elliptical geometry  $(\xi = \frac{r_x}{r_y})$ 

Inverse aspect ratio parameter in slot geometry ( $\zeta =$ 

Centre distance in cylindrical slot geometry (m) b

 $h_i$ Internal convective heat transfer coefficient  $(W/m^2 \cdot K)$ 

Convective heat transfer coefficient on outer tube  $h_o$ surface (W/m<sup>2</sup>·K)

kThermal conductivity of solid or fluid (W/m·K)

Thermal conductivity of air (W/m·K)  $k_a$ 

Thermal conductivity of the wall material (aluminium) (W/m·K)

Thermal conductivity of water (W/m·K)

Number of tubes in the radiator (-)

Semi-major axis of elliptical tube cross-section (m)

Semi-minor axis of elliptical tube cross-section (m)  $r_y$ 

Semi-major axis of elliptical tube inner cross-section

Semi-minor axis of elliptical tube inner cross-section

 $\begin{array}{ll} t & \text{Wall thickness of tube (m)} \\ t_{c,i} & \text{Inlet temperature of cold fluid (K)} \\ t_{c,o} & \text{Outlet temperature of cold fluid (K)} \\ t_{h,i} & \text{Inlet temperature of hot fluid (K)} \\ t_{h,o} & \text{Outlet temperature of hot fluid (K)} \\ u & \text{Mean flow velocity (m/s)} \\ v_o & \text{Velocity of external airflow across the tube (m/s)} \end{array}$ 

## I. INTRODUCTION

UTOMOTIVE thermal management systems rely on compact and efficient heat exchangers, like radiators, to ensure optimal engine performance and prevent overheating. Automotive radiators are typically cross-flow heat exchangers with balanced thermal efficiency and packaging flexibility [1], [2], [3]. In conventional configurations, coolant flows vertically through parallel flat tubes as shown in Fig. 1, while external air is forced perpendicularly (forced convection) across these tubes by vehicle motion and radiator fans. Aluminium is commonly used as the material for the tubes and fins due to its excellent thermal conductivity, corrosion resistance, and ease of manufacturing [4]. The heat transfer process in these radiators primarily involves convective transport from the coolant to the tube walls, conduction through the wall thickness, and convective dissipation to the surrounding air [5], [6], [7].

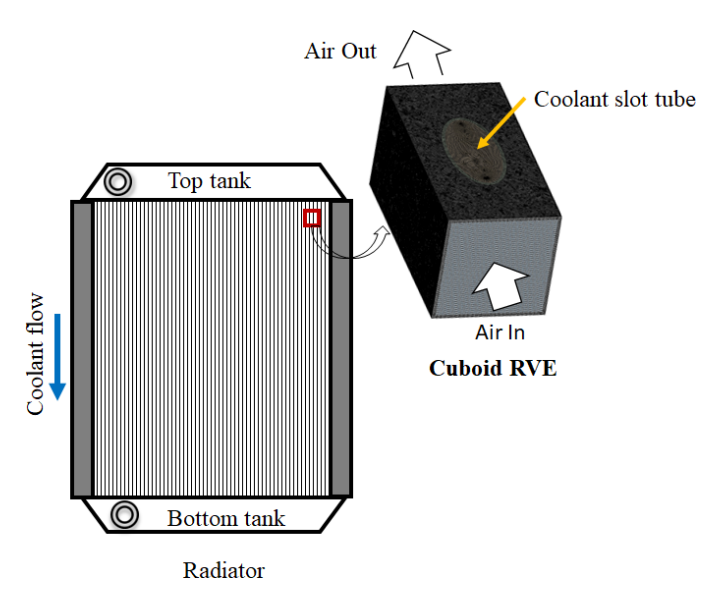


Fig. 1. Schematic of an automotive radiator

In modern automotive radiator design, extruded aluminium flat tubes are commonly used due to their excellent thermal conductivity and lightweight characteristics. The typical wall thickness of these tubes ranges from 0.25 mm to 0.35 mm for passenger cars and light-duty vehicles, while thicker walls up to 0.5 mm are employed in heavy-duty vehicles such as trucks and buses to accommodate higher heat transfer loads [8]. This thin-wall configuration is a trade-off between effective heat transfer, weight reduction, and sufficient structural strength to withstand internal system pressures. Automotive cooling systems operate under elevated pressures, regulated by radiator caps - usually rated between 1.0 and 1.5 bar gauge (equivalent to 2.0–2.5 bar absolute), which raises the boiling point of the coolant significantly [9]. For example, water under 2.0 atm absolute pressure boils around 120°C,

and even higher when mixed with ethylene or propylene glycol, often exceeding 135-140°C. Consequently, radiator tubes must endure sustained internal pressures up to 2.5-3.0 bar absolute without yielding. While the flat tube designs are effective, they might not be the best in terms of pressure drop, surface area utilization, or mechanical strength-toweight ratio. Exploring different tube shapes could lead to better performance. For the tube material, common alloys like AA 6061-T6 and AA3003-H14 exhibiting values in the range of 95-250 MPa are employed. For instance, a stress analysis of a flat tube with a width of 10 mm and a wall thickness of 0.3 mm under an internal pressure of 2 bar indicates a hoop stress of approximately 3.33 MPa, which is well below the yield strength of aluminium alloys [10]. In some of the heat exchanger applications like intercooolers, stainless steel tubes have been employed, which albeit being stronger, increase the weight of the heat exchanger [11]. This confirms the sufficiency of aluminium thin-walled tubes for the radiator applications. Additionally, the pressure drop within these narrow coolant channels, typically ranging from 0.1 to 0.3 bar, remains within acceptable limits and does not impose significant structural stress on the tube walls. Consequently, the combination of material selection, operating pressure strategy, and geometric optimization enables aluminium radiator tubes to achieve high thermal performance while maintaining mechanical robustness and lightweight properties. Elliptical and cylindrical slot-shaped tubes could provide several advantages, such as lower aerodynamic drag, enhanced heat transfer due to their favorable aspect ratios, and improved structural compliance under internal pressure. Despite these potential benefits, these alternative tube designs have not been extensively researched in automotive applications, particularly under real-world conditions that involve two-phase coolant flow and varying air velocities.

This study aims to bridge that gap by developing both analytical thermal resistance models and numerical simulations using ANSYS Fluent to evaluate the performance of elliptical and cylindrical slot tube geometries. Key parameters such as convective heat transfer coefficients, conduction paths, wall thickness requirements, and overall heat transfer resistance are analyzed. The results from the analytical models are validated through CFD simulations under steady-state conditions, incorporating realistic coolant properties and airside flow patterns. The outcomes of this work are expected to inform design optimizations for next-generation radiator tubes with improved thermal efficiency, and mechanical reliability.

## II. METHODOLOGY

## A. Representative Volume Element (RVE) Configuration

To investigate the heat transfer behavior of different tube geometries used in automotive radiators, a Representative Volume Element (RVE) model is established [12]. The RVE consists of a single tube embedded centrally within a cuboidal computational domain. The internal fluid (engine coolant) flows along the tube axis, while the external fluid (air) crosses the tube orthogonally, simulating a crossflow heat exchanger arrangement.

The hot fluid regime is that of the engine coolant. For this, two tube geometries are considered:

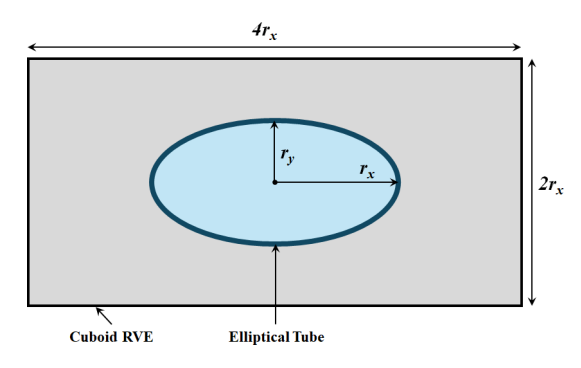


Fig. 2. Geometry of the Elliptical tube within the cuboid RVE

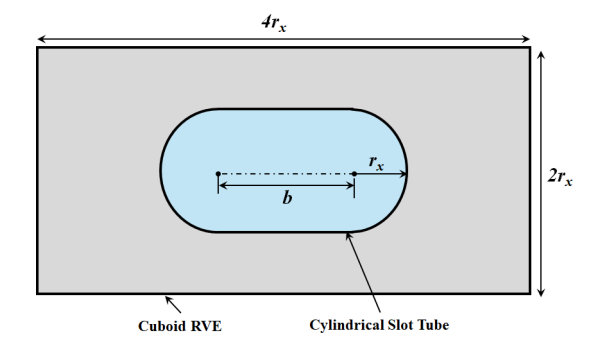


Fig. 3. Geometry of the Cylindrical slot tube within the cuboid RVE

- Elliptical tube: Elliptical cross-section with variable aspect ratio ' $\xi$ ' such that  $\xi = \frac{r_x}{r_y}$ , where  $r_x$  is the major axis and  $r_y$  is the minor axis. This geometry shown in Fig. 2 enhances the surface area perpendicular to external flow and potentially improves thermal performance.
- Cylindrical slot: This geometry shown in Fig. 3 is characterized by a rectangular profile with semicircular ends. The overall shape resembles a capsule or slot and is defined by a radius  $r_x$  (kept same as elliptical cross-section) and a horizontal length b between the semicircles, with aspect ratio  $\zeta$ , such that  $\zeta = \frac{r_x}{b}$ . This design is particularly suited for directional control of the external airflow.

The material for all tube configurations is aluminium, owing to its high thermal conductivity ( $\sim 205~\text{W/m}\cdot\text{K}$ ) [13], corrosion resistance, and manufacturability. Wall thickness of 0.3 mm was considered, balancing heat transfer efficiency and mechanical integrity.

## B. Geometric Considerations and Hydraulic Diameter

The aspect ratios (' $\xi$ ' for elliptical and ' $\zeta$ ' for cylindrical slot) and hydraulic diameter ( $D_h$ ) play a central role in characterizing heat transfer and fluid flow behavior across the different geometries. The hydraulic diameter  $D_h$ , which is one of the key parameters for tube heat exchangers [14], is defined by Eq. 1.

$$D_h = \frac{4A_c}{P_w} \tag{1}$$

where  $A_c$  is the cross-sectional flow area and  $P_w$  is the wetted perimeter. For each geometry:

• Elliptical tube (semi-major axis ' $r_x$ ', semi-minor axis ' $r_y$ '):

$$A_c = \pi r_x r_y \tag{2}$$

The cross-sectional flow area is given by Eq. 2. The expanded perimeter of the elliptical tube is given by Ramanujan's first approximation [15], as shown in Eq. 3, which simplifies to Eq. 4.

$$P_w \approx \pi \left[ 3(r_x + r_y) - \sqrt{(3r_x + r_y)(r_x + 3r_y)} \right] \quad (3)$$

$$P_w = \pi r_x \left[ 3(1 + \frac{1}{\xi}) - \sqrt{(3 + \frac{1}{\xi})(1 + \frac{3}{\xi})} \right]$$
 (4)

The hydraulic diameter is obtained by the simplification as in Eq. 5.

$$D_h = \frac{4A_c}{P_w} = \frac{2\xi^2 r_x}{\left[3(\xi+1) - \sqrt{(3\xi+1)(\xi+3)}\right]}$$
 (5)

• Cylindrical slot (radius of end semicircles  $r_x$ , distance between centers 'b', aspect ratio  $\zeta = \frac{r_x}{b}$ ):

$$A_c = \pi r_x^2 + 2r_x b, \quad P_w = 2\pi r_x + 4b$$
 (6)

$$A_c = \pi r_x^2 + \frac{2r_x^2}{\zeta}, \quad P_w = 2\pi r_x + \frac{4r_x}{\zeta}$$
 (7)

The hydraulic diameter becomes as Eq. 8, and evidently is independent of the aspect ratio  $\zeta$ :

$$D_{h} = \frac{4A_{c}}{P_{w}} = \frac{4r_{x}^{2} \left(\pi + \frac{2}{\zeta}\right)}{2r_{x} \left(\pi + \frac{2}{\zeta}\right)} = 2r_{x}$$
 (8)

## C. Flow Regime and Convective Heat Transfer

Since the coolant is circulated within the engine cooling lines / water jackets utilizing a centrifugal pump, the flow of the coolant is forced [16]. Similarly, the air flow through the radiator is a function of the vehicle speed as well as the suction of the cooling fan mounted behind the radiator. Aptly, the analysis assumes single-phase forced convection on both the internal (coolant) and external (air) sides. The internal flow of the coolant is characterized by the Reynold's number given by Eq. 9.

$$Re_i = \frac{\rho u D_h}{\mu} \tag{9}$$

where ' $\rho$ ' is fluid density, 'u' is mean velocity, ' $D_h$ ' is hydraulic diameter, and ' $\mu$ ' is dynamic viscosity. The coolant discharge capacity of water pumps in car and truck engines typically ranges from 30 to 50 liters per minute, depending on the engine type and operating conditions [17], while industrial coolant pumps can have a discharge up to 350 liters per minute [18]. Assuming a nominal value of 30 L/min for the engine cooling application, the mass flow rate ( $\dot{m}$ ) can be calculated using Eq. 10.

$$\dot{m} = \rho \dot{V} \tag{10}$$

During hot engine operation, the thermostat valve opens fully, allowing the coolant to circulate through the radiator without re-circulating back into the engine. Under this condition, the entire discharge from the pump passes through the radiator coolant tubes. Most automotive radiators contain approximately 30 to 50 tubes, depending on the design and

cooling requirements [19]. Denoting the number of tubes as n, the mass flow through each individual tube can be expressed as Eq. 11. For the current study, the number of tubes n is taken as 50.

$$\dot{m}_{\text{tube}} = \frac{\dot{m}}{n} = \rho u A_c \tag{11}$$

TABLE I Physical and thermal properties of Water between 30 to  $90^{\circ}$ C [20]

| Temperature (°C) | Density<br>(kg/m <sup>3</sup> ) | Dynamic Viscosity (Pa·s) | Thermal conductivity (W/mK) |
|------------------|---------------------------------|--------------------------|-----------------------------|
| 30               | 995.7                           | 0.000797                 | 0.6129                      |
| 40               | 992.2                           | 0.000653                 | 0.6280                      |
| 50               | 988.1                           | 0.000547                 | 0.6397                      |
| 60               | 983.2                           | 0.000466                 | 0.6513                      |
| 70               | 977.8                           | 0.000404                 | 0.6600                      |
| 80               | 971.8                           | 0.000355                 | 0.6687                      |
| 90               | 965.3                           | 0.000315                 | 0.6745                      |

Hence, the Reynold's number can be computed using the modification as in Eq. 12. Referring to Table I, the properties for the hot side fluid (water as coolant) are considered in the temperature range of 30 to 90°C. With  $\rho = 1000 \text{ kg/m}^3$ , n = 50,  $\dot{V} = 30 \text{ L/min}$ , and  $\mu \sim 0.0005 \text{ Pa.s}$ , the mass flow rate through each tube,  $\dot{m}_{\text{tube}} = 0.012 \text{ kg/s}$ , and the Reynold's number can be computed using Eq. 13.

$$Re_i = \frac{\dot{m}_{\text{tube}} D_h}{A_c \mu} = \frac{4\dot{m}_{\text{tube}}}{P_{w_i} \mu} \tag{12}$$

where:

•  $P_{w_i}$  is the wetted perimeter of the inner surface exposed to air

$$Re_i = \frac{96}{P_{w_i}} \tag{13}$$

The coolant flow is then classified as:

• Laminar:  $Re_i < 2300$ • Turbulent:  $Re_i > 4000$ 

For internal forced convection (coolant inside tube), the Nusselt number correlation depends on the flow regime. For fully developed turbulent flow ( $Re_i > 4000$ ), with the hot fluid being cooled, the Dittus-Boelter correlation [21] is applied as given by Eq. 14.

$$Nu_i = 0.023 Re_i^{0.8} Pr_i^{0.3} (14)$$

Once  $Nu_i$  is calculated, the internal convective heat transfer coefficient  $h_i$  is given by Eq. 15.

$$h_i = \frac{Nu_i \cdot k_w}{D_h} \tag{15}$$

For the external crossflow of air over a tube embedded inside a cuboidal domain, the heat transfer coefficient is evaluated using empirical correlations based on the tube geometry and Reynolds number [22]. In this study, the air flows orthogonally across the tube axis, as in a typical radiator setup. For flow over non-circular geometries (like elliptical or cylindrical slot-shaped tubes), these correlations are adapted based on experimental calibration or modified characteristic lengths and of the form shown in Eq. 16.

$$Nu_{o} = C \cdot Re_{o}^{\alpha} \cdot Pr_{o}^{\beta} \tag{16}$$

where:

- C, m, and n are empirical constants depending on geometry and flow regime
- Re<sub>o</sub> is the Reynolds number based on external air flow and hydraulic diameter
- $Nu_o$  is the Nusselt number on the outer surface
- $Pr_o$  is the Prandtl number of air

For flow over non-circular shapes, empirical equations for the Nusselt Number  $Nu_o$  are used. For turbulent flow conditions ( $Re_o > 15000$ ) Eq. 16 takes the form of Eq. 17, where for elliptical shape, the value of  $\alpha = 0.612$  and constant  $C_1 = 0.224$ .

$$Nu_o = 1.1C_1 Re_o^{\alpha} Pr^{\frac{1}{3}} \tag{17}$$

The hydraulic diameter  $D_{h,o}$  for external cross-flow is defined as:

$$D_{h,o} = \frac{4(A - A_c)}{P_{w_c}} \tag{18}$$

where:

- A is the cross-sectional area of the RVE domain perpendicular to the airflow
- $A_c$  is the cross-sectional area occupied by the tube (ellipse or slot)
- $P_{w_o}$  is the wetted perimeter of the outer surface exposed to air

The value of  $(A-A_c)$  accounts for the effective annular space available for airflow and is crucial in evaluating velocity profiles, pressure drop, and heat transfer rates in non-circular tubes. Since the geometry affects both  $A_c$  and  $P_{w_o}$ , the hydraulic diameter and hence the Reynolds number  $Re_o$  vary accordingly.

$$Re_o = \frac{\rho_a u_o D_{h,o}}{\mu_a} \tag{19}$$

where:

- $\rho_a$  is the density of air (kg/m<sup>3</sup>)
- $\bullet$   $u_o$  is the air velocity (external flow) in m/s
- $\mu_a$  is the dynamic viscosity of air (kg/ms)

Once  $Nu_o$  is computed, the external convective heat transfer coefficient  $h_o$  is given by:

$$h_o = \frac{Nu_o \cdot k_a}{D_{h,o}} \tag{20}$$

where  $k_a$  is the thermal conductivity of air.

Elliptical tube: The Prandtl number  $Pr_i$  for water between the temperatures 30°C and 90°C is 3.83. The thermal conductivity of water between the temperature range of 30°C to 90°C is 0.6437 W/mK from Table I. Taking  $r_x$  as 5 mm, and  $\xi=1$  to 10, the different values of  $Re_i$ ,  $Nu_i$  and  $h_i$  are computed as shown in Table II. The values of  $Re_i$  was > 4000, for  $\xi>2$ , which indicated a turbulent flow regime inside the elliptical tube. Since the heat transfer from the coolant has to be maximized, higher values of  $\xi=2$  are advantageous, causing flattening of the elliptical tube. Also, the internal convective heat transfer coefficient  $h_i$  increases significantly with  $\xi$ , as seen in Table II.

TABLE II ELLIPTICAL TUBE : INTERNAL CONVECTIVE HEAT TRANSFER COEFFICIENT  $h_i$  COMPUTED FOR DIFFERENT VALUES OF  $\xi$ 

| ξ  | $P_{w_i}$ | $D_h$  | $Re_i$ | $Nu_i$ | $h_i$      |
|----|-----------|--------|--------|--------|------------|
|    | (m)       | (m)    |        |        | $(W/m^2K)$ |
| 1  | 0.0295    | 0.0106 | 3250.8 | 22.20  | 1343.1     |
| 2  | 0.0228    | 0.0069 | 4216.5 | 27.33  | 2550.0     |
| 3  | 0.0209    | 0.0050 | 4585.0 | 29.23  | 3761.4     |
| 4  | 0.0202    | 0.0039 | 4762.6 | 30.13  | 4977.2     |
| 5  | 0.0197    | 0.0032 | 4861.9 | 30.63  | 6195.8     |
| 6  | 0.0195    | 0.0027 | 4923.4 | 30.94  | 7416.3     |
| 7  | 0.0193    | 0.0023 | 4964.4 | 31.14  | 8638.1     |
| 8  | 0.0192    | 0.0020 | 4993.2 | 31.29  | 9860.7     |
| 9  | 0.0191    | 0.0018 | 5014.3 | 31.39  | 11083.9    |
| 10 | 0.0191    | 0.0016 | 5030.2 | 31.47  | 12307.6    |

TABLE III

PHYSICAL AND THERMAL PROPERTIES OF AIR BETWEEN  $10 \text{ to } 50^{\circ}\text{C}$ [23]

| Temperature | Density              | Dynamic Vis-   | Thermal      |
|-------------|----------------------|----------------|--------------|
| (°C)        | (kg/m <sup>3</sup> ) | cosity (μPa·s) | conductivity |
| , ,         | , ,                  |                | (W/mK)       |
| 10          | 1.247                | 17.65          | 0.02512      |
| 20          | 1.205                | 18.14          | 0.02593      |
| 30          | 1.165                | 18.63          | 0.02675      |
| 40          | 1.128                | 19.12          | 0.02756      |
| 50          | 1.093                | 19.61          | 0.02826      |

Since  $r_x = 5$  mm, the cross-sectional area of the RVE (rectangular) was chosen such that its base was  $2r_x$  and its height was  $4r_x$ . Hence, the rectangle dimensions were 10 mm  $\times$  20 mm, giving an area  $A = 2 \times 10^{-4}$  m<sup>2</sup>. The properties of air between the temperatures of 10°C and 50°C is shown in Table III. For air between 10°C and 50°C, the density  $\rho_a$  is 1.165 kg/m<sup>3</sup>, while thermal conductivity  $k_a$  is 0.02675 W/mK. The Prandtl number for air in the temperature range was considered from Table III( $Pr_o = 0.701$ ). To calculate the effective air velocity  $u_o$ , the vehicle speed  $u_{veh}$  as well as the suction speed due to the cooling fan  $u_{fan}$  have to be considered. Depending on the engine power and size, axial flow fans are utilized with a diameter 0.6 to 0.8 m [24], which can deliver the air discharge rates of 5000 to 10000 ft<sup>3</sup>/min  $(2.36 \text{ to } 4.72 \text{ m}^3/\text{s})$ . Using the continuity equation, the air suction speed due to cooling fans were found to vary between 8.35 m/s and 9.40 m/s. Hence,  $u_{fan}$  was taken as 9 m/s, while the vehicle speed  $u_{veh}$ = 16.7 m/s (at a cruising speed of 60 km/h). Hence,  $u_o = 25.7$  m/s. Using Eq. 17, the external heat transfer coefficient  $h_0$  was computed for different values of  $\xi$  as seen in Table IV. At higher values of  $\xi$ , the value of  $h_o$  was found to decrease since the effective area available for air flow (i.e.  $A - A_c$ ) reduces with increasing values of ξ.

Cylindrical Slot tube: For cylindrical slot tube, using Eq. 13 for internal flow,  $Re_i$  was computed. The expanded perimeter for the inner surface area of the tube  $P_{w,i}$  for this geometry is given by Eq. 21. The corresponding hydraulic diameter  $D_h$  is given by Eq. 22.

$$P_{w,i} = 2(r_x - t)\left(\pi + \frac{2}{\zeta}\right) \tag{21}$$

$$D_h = 2(r_x - t) \tag{22}$$

The values of the internal heat convection are given in Table V. The values of  $Re_i$  was > 2300, for  $\zeta > 2$ , which indicated a transitional flow regime inside the cylindrical slot

TABLE IV ELLIPTICAL TUBE : EXTERNAL CONVECTIVE HEAT TRANSFER COEFFICIENT  $h_o$  COMPUTED FOR DIFFERENT VALUES OF  $\xi$ 

| ξ  | $P_{w_o}$ | $D_{h_o}$ | $Re_o$  | $Nu_o$ | $h_o$      |
|----|-----------|-----------|---------|--------|------------|
|    | (m)       | (m)       |         |        | $(W/m^2K)$ |
| 1  | 0.0314    | 0.0155    | 24853.7 | 107.20 | 185.4      |
| 2  | 0.0242    | 0.0201    | 32236.4 | 125.70 | 167.6      |
| 3  | 0.0223    | 0.0218    | 35054.2 | 132.31 | 162.3      |
| 4  | 0.0214    | 0.0227    | 36411.6 | 135.42 | 159.9      |
| 5  | 0.0210    | 0.0231    | 37171.1 | 137.14 | 158.6      |
| 6  | 0.0207    | 0.0234    | 37641.4 | 138.20 | 157.8      |
| 7  | 0.0206    | 0.0236    | 37954.4 | 138.91 | 157.3      |
| 8  | 0.0205    | 0.0238    | 38174.4 | 139.40 | 157.0      |
| 9  | 0.0204    | 0.0239    | 38335.7 | 139.76 | 156.7      |
| 10 | 0.0203    | 0.0239    | 38457.8 | 140.03 | 156.5      |

tube. With increase in the values of  $\zeta$  from 1 to 10, the internal heat transfer coefficient  $h_i$  was found to increase gradually from 1218 W/m<sup>2</sup>K to 1446 W/m<sup>2</sup>K. Unlike the elliptical slot in which the hydraulic diameter  $D_h$  decreased with  $\xi$ , in case of the cylindrical slot, the hydraulic diameter  $D_h$  remained independent of  $\zeta$ .

TABLE V Cylindrical slot tube : Internal convective heat transfer coefficient  $h_i$  computed for different values of  $\zeta$ 

| ζ  | $P_{w_i}$ | $D_h$  | $Re_i$ | $Nu_i$ | $h_i$      |
|----|-----------|--------|--------|--------|------------|
|    | (m)       | (m)    |        |        | $(W/m^2K)$ |
| 1  | 0.0483    | 0.0094 | 1986.3 | 14.97  | 1024.9     |
| 2  | 0.0389    | 0.0094 | 2465.9 | 17.79  | 1218.5     |
| 3  | 0.0358    | 0.0094 | 2681.7 | 19.03  | 1303.1     |
| 4  | 0.0342    | 0.0094 | 2804.5 | 19.72  | 1350.6     |
| 5  | 0.0333    | 0.0094 | 2883.7 | 20.17  | 1381.0     |
| 6  | 0.0327    | 0.0094 | 2939.0 | 20.48  | 1402.2     |
| 7  | 0.0322    | 0.0094 | 2979.8 | 20.70  | 1417.7     |
| 8  | 0.0319    | 0.0094 | 3011.2 | 20.88  | 1429.7     |
| 9  | 0.0316    | 0.0094 | 3036.1 | 21.02  | 1439.1     |
| 10 | 0.0314    | 0.0094 | 3056.3 | 21.13  | 1446.8     |

In case of the cylindrical slot, for the external air flow, the dimensions of the rectangular cross-section of the RVE is kept same as that taken up for the elliptical tube  $(2 \times 10^{-4} \text{ m}^2)$ . The expanded perimeter for the outer surface area of the tube  $P_{w,o}$  for this geometry is given by Eq. 23.

$$P_{w,o} = 2(r_x) \left( \pi + \frac{2}{\zeta} \right) \tag{23}$$

Hence, the hydraulic diameter for external cross-flow is given by Eq. 24, which simplifies to Eq. 25.

$$D_{h,o} = \frac{4(A - A_c)}{P_{w_o}} = \frac{4(8r_x^2 - \pi r_x^2 - 2br_x)}{P_{w_o}}$$
 (24)

$$D_{h,o} = \frac{4r_x^2(8 - \pi - \frac{2}{\zeta})}{P_{w_o}} \tag{25}$$

The values of the external heat transfer coefficient  $h_o$  for the cylindrical slot are tabulated in Table VI. With increase in  $\zeta$ , the convective heat transfer coefficient decreased from 225.7 W/m<sup>2</sup>K to 193 W/m<sup>2</sup>K. The convective coefficients in case of the cylindrical slot tubes were larger than those observed for the elliptical tubes.

## D. Thermal Resistance Network

The overall heat transfer through a single tube within the RVE is modeled using a thermal resistance network consisting of three primary components:

TABLE VI CYLINDRICAL SLOT TUBE : EXTERNAL CONVECTIVE HEAT TRANSFER COEFFICIENT  $h_o$  COMPUTED FOR DIFFERENT VALUES OF  $\zeta$ 

| ζ  | $P_{w_o}$ | $D_{h_o}$ | $Re_o$  | $Nu_o$ | $h_o$      |
|----|-----------|-----------|---------|--------|------------|
|    | (m)       | (m)       |         |        | $(W/m^2K)$ |
| 1  | 0.0514    | 0.0056    | 8934.5  | 57.32  | 275.8      |
| 2  | 0.0414    | 0.0093    | 14972.2 | 78.61  | 225.7      |
| 3  | 0.0381    | 0.0110    | 17689.4 | 87.06  | 211.6      |
| 4  | 0.0364    | 0.0120    | 19234.6 | 91.64  | 204.8      |
| 5  | 0.0354    | 0.0126    | 20231.5 | 94.52  | 200.8      |
| 6  | 0.0347    | 0.0130    | 20927.9 | 96.49  | 198.2      |
| 7  | 0.0343    | 0.0133    | 21442.0 | 97.94  | 196.4      |
| 8  | 0.0339    | 0.0136    | 21837.0 | 99.04  | 195.0      |
| 9  | 0.0336    | 0.0138    | 22150.1 | 99.90  | 193.9      |
| 10 | 0.0334    | 0.0139    | 22404.2 | 100.60 | 193.0      |
|    |           |           |         |        |            |

- **Internal convection resistance** due to forced convection from the coolant to the inner tube wall.
- Conduction resistance through the aluminum tube wall.
- External convection resistance due to cross-flow of air over the outer tube surface.

Elliptical Tube: For the elliptical tube with major axis  $r_x$ , minor axis  $r_y$ , wall thickness t, and tube length L, the inner semi-major and semi-minor axes are given as:  $r_{x,i} = r_x - t$ ,  $r_{y,i} = r_y - t$ .

The thermal resistance components for the hot fluid (inside the tube) are:

$$R_{conv,i} = \frac{1}{h_i P_{w,i} L} \tag{26}$$

$$R_{cond} = \frac{1}{2\pi k_t L} \ln \left( \frac{r_x r_y}{r_{x,i} r_{y,i}} \right) \tag{27}$$

$$R_{cond} = \frac{1}{\pi k_t L} \ln \left( \frac{r_x}{r_x - t} \right) \tag{28}$$

$$R_{conv,o} = \frac{1}{h_o P_{w,c} L} \tag{29}$$

Based on Eq. 4, the expanded perimeter  $P_{w_o}$  for the outer tube side is given by Eq. 30, while for the inner tube side,  $P_{w_i}$  is given by Eq. 31.

$$P_{w_o} = \pi r_x \left[ 3(1 + \frac{1}{\xi}) - \sqrt{(3 + \frac{1}{\xi})(1 + \frac{3}{\xi})} \right]$$
 (30)

$$P_{w_i} = \pi(r_x - t) \left[ 3(1 + \frac{1}{\xi}) - \sqrt{(3 + \frac{1}{\xi})(1 + \frac{3}{\xi})} \right]$$
 (31)

Cylindrical Slot Tube: For a cylindrical slot geometry, the same wall thickness t, wall material as aluminium with thermal conductivity  $k_t \ (= 205 \ \text{W/mK})$  and length L as that of the above case is considered. The slot comprises two semicircular ends (of radius  $r_x$  with centre-to-centre separated of b) and two flat walls on opposite sides.

The different thermal resistances are given by:

$$R_{conv,i} = \frac{1}{h_i L} \left[ \frac{1}{2\pi (r_x - t)} + \frac{2\zeta}{r_x} \right]$$
 (32)

$$R_{conv,o} = \frac{1}{h_o r_x L} \left[ \frac{1}{2\pi} + 2\zeta \right] \tag{33}$$

$$R_{cond,f} = \frac{2t}{k_t \frac{r_x}{\zeta} L} = \frac{2\zeta t}{k_t r_x L}$$
 (34)

$$R_{cond,c} = \frac{1}{2\pi k_t L} \ln \left[ \frac{r_x}{(r_x - t)} \right]$$
 (35)

$$R_{cond,tot} = \frac{2\zeta t}{k_t r_x L} + \frac{1}{2\pi k_t L} \ln \left[ \frac{r_x}{r_x - t} \right]$$
 (36)

The total resistance expressions are then:

$$R_{\text{tot,ellipse}} = \frac{1}{h_i P_{w_i} L} + \frac{1}{\pi k_t L} \ln \left( \frac{r_x}{r_x - t} \right) + \frac{1}{h_i P_{w_o} L}$$
(37)

$$R_{
m tot,slot} pprox \left(rac{1}{h_i(r_x - t)L} + rac{1}{h_o r_x L}
ight) \left[rac{1}{2\pi} + 2\zeta
ight] + R_{cond,tot}$$
 (38)

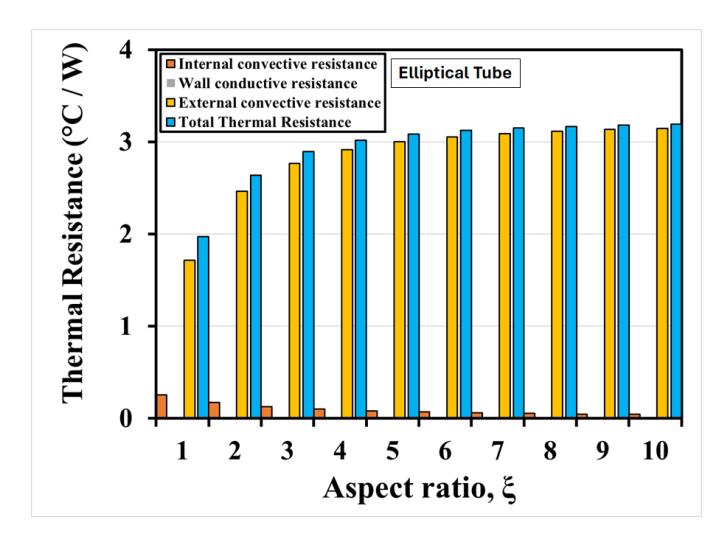


Fig. 4. Variation of the total thermal resistance of the elliptical tube with  $\varepsilon$ 

For the elliptical tube, the values of the total thermal resistance at different values of  $\xi$  are shown in Fig. 4. As  $\xi$  increases, the total thermal resistance was also found to increase, which was strongly dependent on the external convective resistance of the air. The internal convective resistance of water was found to decrease with increasing values of  $\xi$ , while the thermal conductive resistance of the wall was negligible at 0.00096 °C /W at all values of  $\xi$ . It is interesting to note that the tube becomes flatter as  $\xi$  increases, but at the same time, the total thermal resistance also was found to increase. Beyond  $\xi = 4$ , the total thermal resistance stabilized at  $\sim$  3 °C /W.

For the cylindrical slot tube, the values of the total thermal resistance at different values of  $\zeta$  are shown in Fig. 5. As  $\zeta$  increased, the total thermal resistance increased drastically, due to a rapidly increasing external convective resistance of the air. The total thermal resistance at  $\zeta=10$  was 236.7 °C /W, which indicated a poor heat transfer across the cylindrical slot tube. Since at  $\zeta=2$ , the total thermal resistance of the cylindrical slot tube was ten times that of the elliptical tube, hence lower values of  $\zeta<1$  were further studied. At  $\zeta=0.45$ , the total thermal resistance of the cylindrical slot tube dropped to 5.97 °C/W, which was still twice the total thermal resistance of elliptical tubes at  $\xi>4$ . The internal convective resistance of water was also found to increase with increasing values of  $\zeta$ , while the thermal conductive resistance of the wall was negligible compared to the other

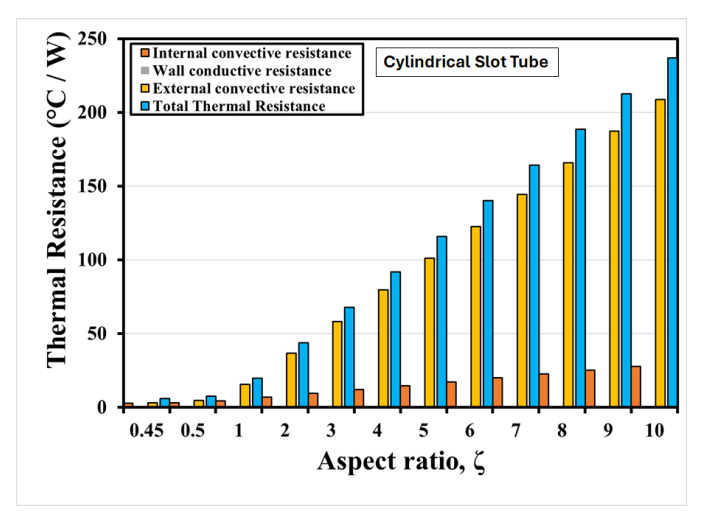


Fig. 5. Variation of the total thermal resistance of the cylindrical slot tube with  $\boldsymbol{\zeta}$ 

resistances. However, the thermal conductive resistance was found to increase with an increase in  $\zeta$  reaching 0.06 °C/W at  $\zeta = 10$  from 0.003 at  $\zeta = 0.45$ .

#### III. NUMERICAL MODELLING

The elliptical tube performed better than the cylindrical slot tube in terms of the total thermal resistance. Hence, the elliptical tube was chosen for the numerical analysis. The geometry of the Elliptical slot within the cuboid RVE is shown in Fig. 6, earmarking the hot and cold fluid domains respectively. The 3D numerical model of the elliptical tube within the cuboid RVE was setup in ANSYS® Fluent software as shown in Fig. 7. For the elliptical tube  $r_x = 5$ mm,  $r_y = 2.5$  mm, such that  $\xi = 2$ . For the cuboid RVE, the dimensions were 4  $r_x$   $\times$  2  $r_x$   $\times$  2  $r_x$ . A mesh sizing of 0.1 mm was employed for the hot domain (water) and the cold domain (air). For the tube walls, and RVE walls, a mesh size of 0.2 mm was employed. Water flowed through the elliptical tube, while air passed through the recess of the cuboid RVE between the square outer cross-section and the inner tubular space.

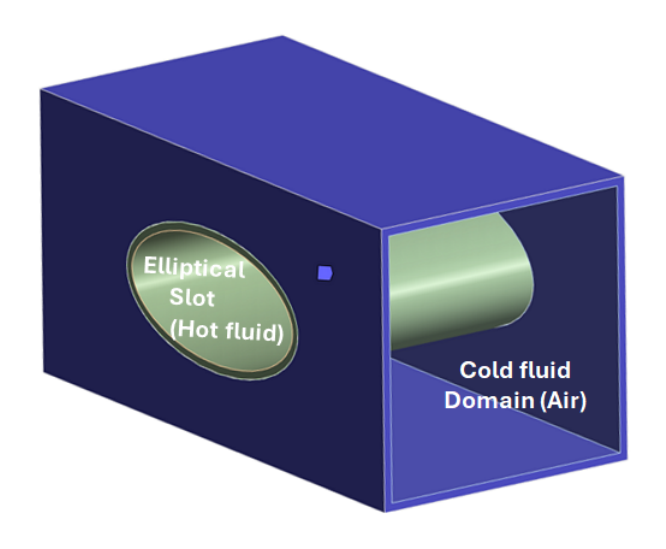


Fig. 6. Geometry of the Elliptical slot carrying hot fluid and Annular space of cuboid RVE for flow of cold fluid

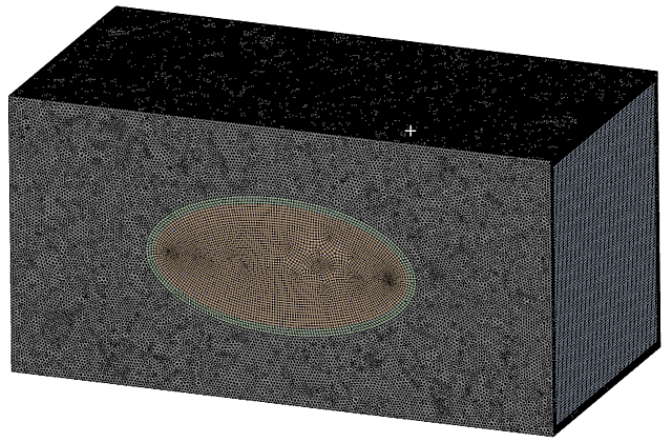


Fig. 7. Numerical model of the elliptical tube within the cuboid RVE

For the solver, the energy model was kept in on condition, with the viscous model being realizable k- $\epsilon$  turbulence model. The turbulent Prandtl numbers  $\sigma_k = 1.0$ ,  $\sigma_{\varepsilon} = 0.85$ , and the components of rate of deformation were  $C_{1\varepsilon} = 1.44$ , and  $C_{2\varepsilon} = 1.92$ . To reduce computational effort, the enhanced wall function approach was used, which avoids the need to resolve the complex near-wall region. Based on the mass flow rates of air and water taken up in the analytical approach,  $\dot{m}_a = 4.96 \times 10^{-3}$  kg/s, while  $\dot{m}_{tube} = 0.012$ kg/s. The inlet temperature of air was taken as 25 °C (298 K), while the inlet temperature of water was taken as 100 °C (373 K). The flow conditions were updated in the computational fluid dynamics model shown in Fig. 8. The outlet conditions for the air as well as water were kept as outflow in the solver. The temperature distribution, velocity vectors across the cold domain (air) and hot domain (water), along with the surface heat flux were recorded.

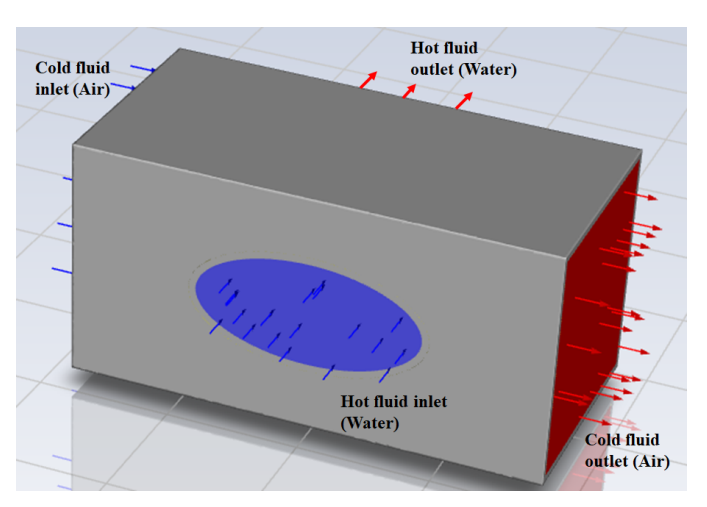


Fig. 8. The flow conditions for the air and coolant employed within the RVE / elliptical tube

The temperature distribution at the outlet of the hot fluid (water) is shown in Fig. 9. The area-averaged outlet temperature of water was computed as 318.12 K. The temperature distribution at the outlet of the cold fluid (air) is shown in Fig. 10. The area-averaged outlet temperature of air was found to be 310.10 K. For counterflow heat exchangers, the logarithmic mean temperature difference (LMTD) is given by Eq. 39. For cross-flow heat exchangers like the

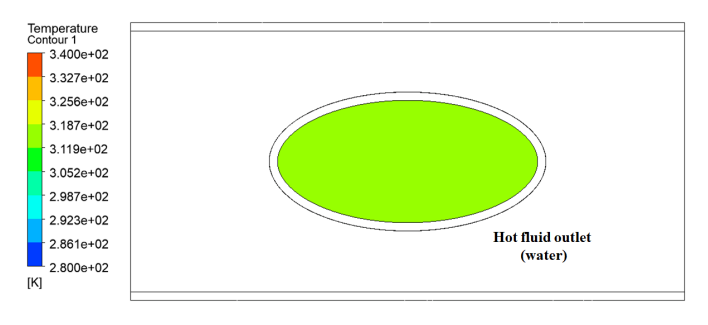


Fig. 9. Temperature distribution at the hot fluid outlet (water)

one considered in the above work, a correction factor F is considered along with LMTD, based on Bowman charts [25]. For the current heat exchanger, a single fluid mixed (air) and other fluid unmixed (water) were considered. For the temperature values of the air and water for the cross flow heat exchanger, the correction factor F was found to be 0.85. The LMTD  $\theta_m = 37.53$  K. Incorporating the correction factor, corrected temperature difference  $\theta_{cf} = 31.90$  K.

$$\theta_m = \frac{(t_{h,i} - t_{c_o} - t_{h,o} + t_{c,i})}{ln\frac{(t_{h,i} - t_{c_o})}{(t_{h,o} - t_{c,i})}}$$
(39)

$$\theta_{cf} = F\theta_m \tag{40}$$

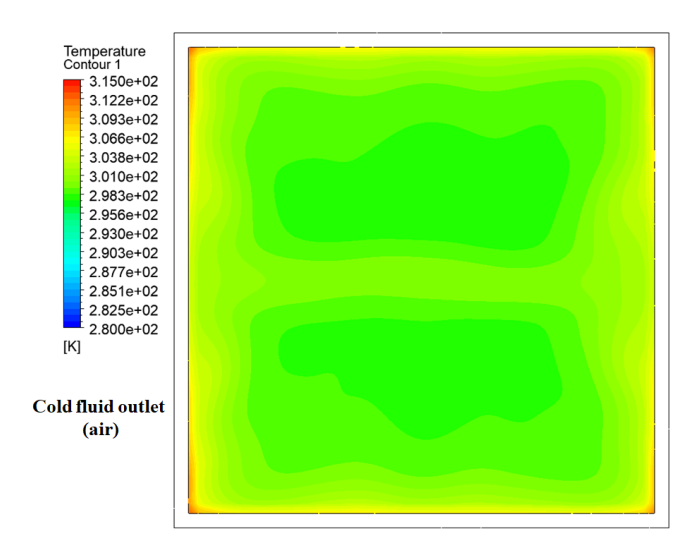


Fig. 10. Temperature distribution at the cold fluid outlet (air)

The rate of heat transfer across the cross-flow heat exchanger was evaluated using Eq. 41, which relates the heat flux to the overall heat transfer coefficient and the effective surface area of the tube. The spatial distribution of total heat flux along the inner surface of the elliptical tube wall is depicted in Fig. 11. The simulation revealed a peak local heat flux of 1.24 MW/m², while the area-averaged heat flux was found to be 0.318 MW/m², indicating significant non-uniformity due to local flow field variations and thermal boundary layer development. The corresponding thermal resistance of the tubular wall was computed based on the relation  $\frac{1}{UA_c}$ , where U is the overall heat transfer coefficient and  $A_c$  is the curved area of the elliptical tube, obtained from Eq. 2. Substituting the appropriate values from simulation results into Eq. 41, the thermal resistance was

determined to be 2.553 °C/W. For comparison, an analytical estimation of the total thermal resistance for the elliptical configuration yielded  $R_{\rm tot,ellipse}=2.636$  °C/W. The close agreement between the numerical and analytical results, with a relative deviation of only 3.15%, validates the accuracy of the numerical model and the robustness of the simulation methodology adopted. This also reinforces the reliability of using CFD-assisted thermofluid simulations for predicting performance metrics in advanced heat exchanger designs.

$$\dot{q}_{cf} = U\theta_{cf} \tag{41}$$

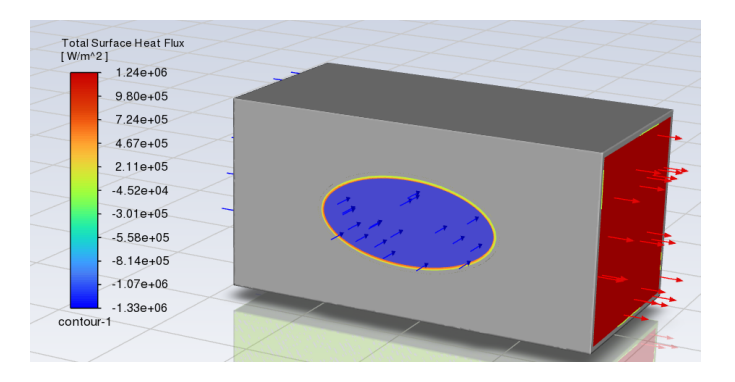


Fig. 11. Surface Heat Flux distribution across the tubular surface

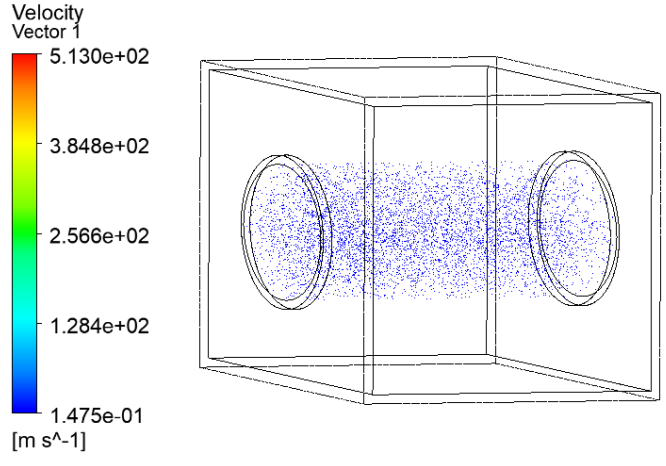


Fig. 12. Velocity vector plot of the hot fluid domain (water)

Fig. 12 presents the velocity vector distribution for the hot fluid domain (water), whereas Fig. 13 illustrates the same for the cold fluid domain (air). In the air domain, the presence of the tubular structure introduces a geometric obstruction that alters the flow field, as seen in Fig. 10(a). This structural interference induces non-uniformity in the velocity contours across the flow domain. Notably, at the outlet of the cold fluid region, elevated velocity magnitudes are concentrated near the central axis of the outlet face, as shown in Fig. 13(b), indicating accelerated flow through the central region where the tubular sectional area is maximum.

#### IV. CONCLUSIONS

The study compared the thermal performance of elliptical and cylindrical slot tube geometries in a cross-flow heat exchanger configuration for automotive radiator applications.

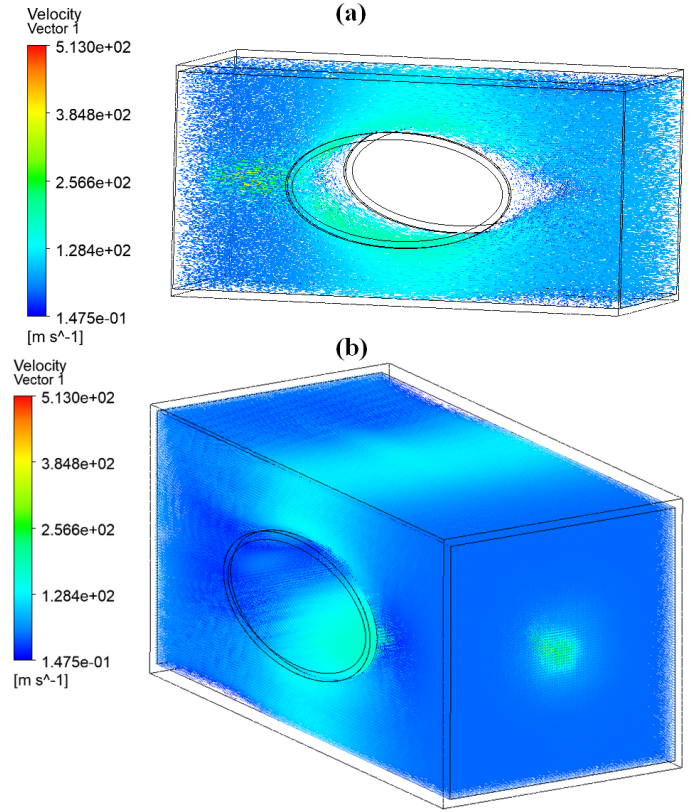


Fig. 13. Velocity vector plot of the cold fluid domain (air) (a) Side view (b) Peripheral view

Elliptical tubes consistently exhibited lower total thermal resistance, with values stabilizing around 3 °C/W for higher aspect ratios ( $\xi>4$ ). In contrast, cylindrical slot tubes showed much higher resistance, especially at larger  $\zeta$  values, indicating poor heat transfer efficiency. A validated CFD simulation for an elliptical tube at  $\xi=2$  yielded a thermal resistance of 2.553 °C/W, closely matching the analytical value of 2.636 °C/W. These results support the use of elliptical tube profiles for thermally efficient automotive radiator designs.

#### REFERENCES

- [1] K. W. Park and H. Y. Pak, "Flow and heat transfer characteristics in flat tubes of a radiator," *Numerical Heat Transfer: Part A: Applications*, vol. 41, no. 1, pp. 19–40, 2002.
- [2] E. Keklik and M. Hoşöz, "Comparison of the experimental performance of round and flat tube automobile radiators for various coolants," *Politeknik Dergisi*, vol. 23, no. 4, pp. 1121–1130, 2020.
- [3] W. E. Ukueje, F. I. Abam, and A. Obi, "A perspective review on thermal conductivity of hybrid nanofluids and their application in automobile radiator cooling," *Journal of Nanotechnology*, vol. 1, no. 2187932, pp. 1–51, 2022.
- [4] A. Witry, M. H. Al-Hajeri, and A. A. Bondok, "Thermal performance of automotive aluminium plate radiator," *Applied Thermal Engineering*, vol. 25, no. 8-9, pp. 1207–1218, 2005.
- [5] F. W. Dittus and L. M. K. Boelter, "Heat transfer in automobile radiators of the tubular type," *International Communications in Heat* and Mass Transfer, vol. 12, no. 1, pp. 3–22, 1985.
- [6] M. I. Azis, "Numerical investigation for unsteady heat conduction problems of anisotropic trigonometrically graded materials," *Engineering Letters*, vol. 31, no. 4, pp. 1700–1706, 2023.
- [7] M. I. Azis, "A simulation of unsteady heat conduction problems for anisotropic quadratically graded materials," *Engineering Letters*, vol. 31, no. 4, pp. 1134–1140, 2023.
- [8] F. Neves, A. A. Soares, and A. Rouboa, "Forced convection heat transfer of nanofluids in turbulent flow in a flat tube of an automobile radiator," *Energy Reports*, vol. 8, no. 9, pp. 1185–1195, 2022.

- [9] D. Arunpandiyan et al., "A review of automotive radiator performance," International Journal for Innovative Research in Science & Technology, vol. 2, no. 10, pp. 166–169, 2016.
- [10] T. Trzepieciński, S. M. Najm, V. Oleksik, D. Vasilca, I. Paniti, and M. Szpunar, "Recent developments and future challenges in incremental sheet forming of aluminium and aluminium alloy sheets," *Metals*, vol. 12, no. 1, pp. 1–46, 2022.
- [11] A. Arifin, I. Yani, H. Irawan, et al., "Failure analysis of 304 stainless steel tubes of intercooler carbon dioxide compressor," Engineering Letters, vol. 31, no. 1, pp. 159–164, 2023.
- [12] A. Takezawa, X. Zhang, and M. Kitamura, "Optimization of an additively manufactured functionally graded lattice structure with liquid cooling considering structural performances," *International Journal of Heat and Mass Transfer*, vol. 143, no. 118564, pp. 1–17, 2019.
- [13] A. Zhang and Y. Li, "Thermal conductivity of aluminum alloys—a review," *Materials*, vol. 16, no. 2972, pp. 1–21, 2023.
- [14] A. A. Bhuiyan and A. K. M. Sadrul Islam, "Thermal and hydraulic performance of finned-tube heat exchangers under different flow ranges: A review on modeling and experiment," *International Journal* of Heat and Mass Transfer, vol. 101, pp. 38–59, 2016.
- [15] P. Moscato and A. Ciezak, "A new approximation for the perimeter of an ellipse," *Algorithms*, vol. 17, no. 10, pp. 1–15, 2024.
- [16] H. Wang, Y. Zhou, X. Li, X. Wu, H. Wang, A. Elnaz, K. Granlund, R. Lahdelma, and E. Teppo, "Study on the performance of a forced convection low temperature radiator for district heating," *Energy*, vol. 283, no. 129036, pp. 1–13, 2023.
  [17] M. L. M. Tasuni, Z. A. Latiff, H. Nasution, M. R. M. Perang,
- [17] M. L. M. Tasuni, Z. A. Latiff, H. Nasution, M. R. M. Perang, H. M. Jamil, and M. N. Misseri, "Performance of a water pump in an automotive engine cooling system," *Jurnal Teknologi (Sciences & Engineering)*, vol. 78, no. 10-2, pp. 47–53, 2016.
- [18] M. Fang, J. Tang, and P. Zhou, "Analysis on the pump selection in the reconstruction of the cooling water system at Chinese High Magnetic Field Laboratory," *Engineering Letters*, vol. 32, no. 8, pp. 1616–1622, 2024.
- [19] N. Vinukonda and V. K. Sharma, "Review on contemporary trends in radiator design and testing of automobile radiators," *International Journal of Mechanical Engineering and Technology*, vol. 9, no. 12, pp. 671–680, 2018.
- [20] J. Brodholt and B. Wood, "Simulations of the structure and thermodynamic properties of water at high pressures and temperatures," *Journal* of Geophysical Research: Solid Earth, vol. 98, no. B1, pp. 519–536, 1993.
- [21] H. Li, A. Kruizenga, M. Anderson, M. Corradini, Y. Luo, H. Wang, and H. Li, "Development of a new forced convection heat transfer correlation for CO2 in both heating and cooling modes at supercritical pressures," *International Journal of Thermal Sciences*, vol. 50, no. 12, pp. 2430–2442, 2011.
- [22] A. Horvat, M. Leskovar, and B. Mavko, "Comparison of heat transfer conditions in tube bundle cross-flow for different tube shapes," *International Journal of Heat and Mass Transfer*, vol. 49, no. 5-6, pp. 1027–1038, 2006.
- [23] P. T. Tsilingiris, "Thermophysical and transport properties of humid air at temperature range between 0 and 100 C," *Energy Conversion* and *Management*, vol. 49, no. 5, pp. 1098–1110, 2008.
- [24] R. Nageswara, K. Sukhvinder, K. Ravi, and K. Niranjan, "CFD analysis of axial flow fans for radiator cooling in automobile engines," SAE Technical Paper, vol. 4262, no. 1, pp. 1–9, 2007.
- [25] R. A. Bowman, "Mean temperature difference correction in multipass exchangers," *Industrial & Engineering Chemistry*, vol. 28, no. 5, pp. 541–544, 1936.